Physics of the Earth and Planetary Interiors 317 (2021) 106749

Contents lists available at ScienceDirect

Physics of the Earth and Planetary Interiors

journal homepage: www.elsevier.com/locate/pepi

Marsquakes

Refining geomagnetic field intensity changes in Europe between 200 CE and 1800 CE. New data from the Mediterranean region

M. Rivero-Montero [a,*], M. Gómez-Paccard [a], F.J. Pavón-Carrasco [b], M.A. Cau-Ontiveros [c,d], L. Fantuzzi [d,e], F. Martín-Hernández [a,b], A. Palencia-Ortas [a,b], E. Aidona [f], E. Tema [g,h], D. Kondopoulou [f], C. Mas-Florit [d], J. Ramon-Torres [i]

[a] Instituto de Geociencias (IGEO) CSIC, UCM, c/Doctor Severo Ochoa, 7. Facultad de Medicina (edificio entrepabellones 7-8), Ciudad Universitaria, 28040 Madrid, Spain
[b] Dpto. de Física de la Tierra, Astronomía y Astrofísica I, Universidad Complutense de Madrid (UCM), Avd. Complutense s/n, 28040 Madrid, Spain
[c] ICREA, Pg. Lluís Companys 23, 08010 Barcelona, Spain
[d] Equip de Recerca Arqueològica i Arqueomètrica de la Universitat de Barcelona (ERAAUB), Institut d'Arqueologia de la Universitat de Barcelona (IAUB), Departament d'Història i Arqueologia, Facultat de Geografia i Història, Universitat de Barcelona (UB), c/Montalegre, 6, 08001 Barcelona, Spain
[e] Universidad de Cádiz, Spain
[f] Aristotle University of Thessaloniki, Department of Geophysics, School of Geology, 54124 Thessaloniki, Greece
[g] Università degli Studi di Torino, Dipartimento di Scienze della Terra, Via Valperga Caluso 35, 10125 Torino, Italy
[h] Alpine Laboratory of Paleomagnetism ALP-CIMaN, Via G.U. Massa 6, 12016 Peveragno, Italy
[i] Consell Insular d'Eivissa, Spain

ARTICLE INFO

Keywords:
Archeomagnetism
Archeointensity
Geomagnetic field strength maxima
Paleomagnetism
Mediterranean

ABSTRACT

Absolute past geomagnetic intensity values can mainly be recovered by fired archaeological materials and volcanic rocks. Here, we present 10 new archeointensities from the Mediterranean region that help to better constrain geomagnetic field intensity changes in Europe over the last two millennia. The new archeointensity results were obtained from the Thellier classical method including thermoremanent magnetization (pTRM) checks and both the TRM anisotropy and cooling rate corrections and were derived from at least three specimens. The new data presented, together with a selection of previous archeointensities satisfying a set of quality criteria, confirm the presence of several intensity maxima in Europe over the last 2000 years. In particular, the new archeointensities allow to better define the starting point of the double-oscillation feature that occurred in Europe during the second half of the first millennium CE, and reinforce the existence of a relative maximum at the end of the 14th century - beginning of the 15th century in Western Europe. From selected European archeointensities two new paleosecular variation curves are constructed for Western and Eastern Europe using temporal cubic b-splines in a bootstrap approach. The obtained curves suggest that the occurrence of the intensity maxima is characterized by a period of about 300 ± 50 years. In addition, our results suggest that the maxima do not occur simultaneously in Western and Eastern Europe, pointing out an intensity eastward drift with a mean lag-time of about 100 years.

1. Introduction

Nowadays, it is well known that the past geomagnetic field strength has exhibited numerous intense, short-lived (multidecadal) maxima at different times and locations (eg., Ben-Yosef et al., 2009; Shaar et al., 2011, 2016; among others). In Europe, several archeomagnetic studies conducted over the past few decades resulted in a refined description of geomagnetic field intensity changes over the last few millennia at regional scales (e.g., Genevey et al., 2016, 2018, 2019; Gómez-Paccard et al., 2012, 2016; Kovacheva et al., 2014; Rivero-Montero et al., 2021; Schnepp et al., 2020; Tema et al., 2010, 2012). These studies confirmed that several relative intensity maxima and minima were achieved in

* Corresponding author.
E-mail addresses: m.rivero@csic.es (M. Rivero-Montero), mgomezpaccard@csic.es (M. Gómez-Paccard), fjpavon@ucm.es (F.J. Pavón-Carrasco), macau@ub.edu (M.A. Cau-Ontiveros), leandro.fantuzzi@uca.es (L. Fantuzzi), fatima@ucm.es, ali@ucm.es (F. Martín-Hernández), aidona@geo.auth.gr (E. Aidona), evdokia.tema@unito.it (E. Tema), despi@geo.auth.gr (D. Kondopoulou), cmas@ub.edu (C. Mas-Florit).

https://doi.org/10.1016/j.pepi.2021.106749
Received 2 February 2021; Received in revised form 19 May 2021; Accepted 27 May 2021
Available online 29 May 2021
0031-9201/© 2021 Elsevier B.V. All rights reserved.

Europe over the past 2000 years but the specific pattern of oscillations is still a matter of debate (e.g., Kovacheva et al., 2014; Genevey et al., 2016; Gómez-Paccard et al., 2016).

For Western Europe, the study of Genevey et al. (2016) is one of the most detailed available studies on this topic. These authors, based on a selection of archeointensities within an area of 700 km around Paris, suggested that the geomagnetic field exhibited five intensity maxima over the last 1500 years. These maxima were located at the transition between the 6th and the 7th century CE, at the middle of the 9th century, during the 12th century, in the second part of the 14th century and at the very beginning of the 17th century CE. They also pointed out that some of the peaks are smoothed or nearly absent when the selection of data is extended to a larger region of 1250 km of radius around Paris. Almost contemporaneously, Gómez-Paccard et al. (2016), using a different selection of high-quality intensity data from France, Spain, Portugal, Switzerland and Belgium, proposed a similar oscillation trend but with some differences in the maximum values achieved during some of the bumps (e.g., for the peak achieved around 600 CE) or in the occurrence time of each peak (e.g., a short intensity peak is recorded around 1300 CE in the bootstrap curve, but observed about 50 yr later in the Bayesian curve proposed in that study or in the work of Genevey et al., 2016). In any case, both studies highlighted the importance of data selection for properly reconstructing the past behavior of the geomagnetic field intensity, as is has also been recognized in other publications (Chauvin et al., 2000; Genevey et al., 2008, 2019; Gómez-Paccard et al., 2012; Pavón-Carrasco et al., 2014; among others).

Among the different peaks identified in Western Europe, the most important intensity feature depicted is the double-oscillation that occurred during the second half of the first millennium CE and is characterized by the highest intensities of the last two millennia (Genevey and Gallet, 2002; Genevey et al., 2016; Gómez-Paccard et al., 2008, 2012, 2016). This double-oscillation has also been identified in the intensity paleosecular variation (PSV) curve proposed for Bulgaria (Kovacheva et al., 2014), and from different selections of data from Bulgaria, Greece and Italy (Gómez-Paccard et al., 2012, 2016; Genevey et al., 2016, 2018). However, it is not well recovered in other European regions due to the low number of available archeointensity data covering this period and/or due to the large scatter in the available results. This is the case of Iberia, Germany and Finland, among other regions. In the Iberian Peninsula, the last PSV curve centered at Madrid, which also includes some data from southern France and northern Morocco, does not show the double-oscillation but indicates high intensity values between the 5th and 9th centuries CE (Molina-Cardín et al., 2018). After that, a slow decrease in intensity is observed with almost no evidence of oscillations after 1000 CE (see also Genevey et al., 2019 for a discussion). In Germany (Schnepp et al., 2020) and Finland (Pesonen et al., 1995) high intensities have also been obtained for this period, but the double-oscillation is not well recognized by the few data available.

Therefore, and despite the great effort made in the previously mentioned studies, the spatial and temporal extension of the intensity maxima in Europe is not well constrained. For instance, an important unresolved question is if the different maxima are simultaneously observed all over Europe or not (Gómez-Paccard et al., 2012, 2016; Molina-Cardín et al., 2018; Genevey et al., 2016, 2019; Schnepp et al., 2020). In this context, new data are essential to gain insight into the geomagnetic field evolution in Europe over the last 2000 years. This contribution is part of this general effort and we present a complete archeomagnetic study of fired archaeological materials collected in six different archaeological sites located in Spain, Italy, and Greece (Fig. 1).

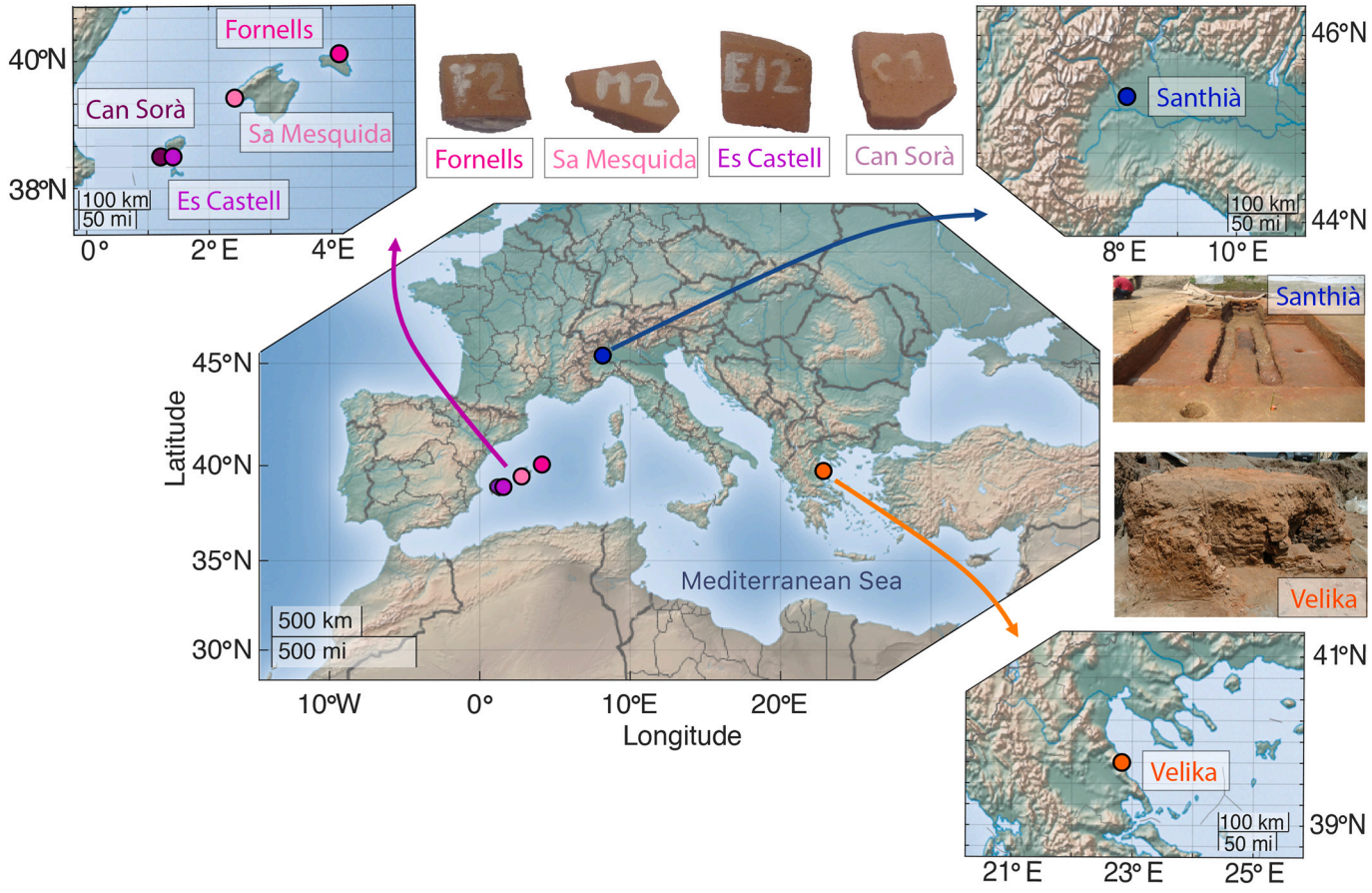

Fig. 1. Location of the six archaeological sites where the archaeological materials were recovered, and pictures of representative potteries and kilns studied.

2. Materials

The studied collection includes 53 ceramic fragments, six tiles and two kilns collected in six sites from Spain, Italy, and Greece (Fig. 1). In Spain, 53 samples of utilitarian ceramics (mainly some common buff wares but also a few amphorae), collected from the rims of the vessels to have a precise typological classification, were selected from four different archaeological sites in the Balearic Islands representing four archaeological deposits dated to 400–625 CE: Sa Mesquida (Mallorca), Es Castell (Ibiza), Can Sorà (Ibiza), and Fornells (Menorca). In Italy, 12 brick samples from a kiln dated back to 1490–1574 CE were selected at the site of Santhià. Finally, in Greece, from an archaeological site located near Velika, we selected six unoriented samples from the walls of a kiln dated to the 6th century CE and six large roof tiles from its production. Macroscopically, the studied ceramics are fine-grained fragments fairly homogeneous in their composition with no distinctive inclusions. The tiles and kiln's samples were red clays fired at high temperatures. The specific details of the archaeological context and dating of the studied material are provided below.

2.1. Sa Mesquida (Mallorca)

Sa Mesquida (MC) is a Roman rural settlement located in Santa Ponça, Calvià, in western Mallorca (Balearic Islands) (Mas Florit et al., 2015). The site was probably founded in the time of Augustus (27 BCE-14 BCE) and partially destroyed at the end of the 2nd or earlier 3rd century but shows also Late Antique phases of occupation. Precisely, the studied ceramics were found in a Roman cistern that was later used as a rubbish dump in Late Antiquity. The deposit contained large quantities of regional and imported ceramics including buff common wares (many from the neighboring island of Ibiza), cooking wares, amphorae, fine tableware, and other materials such as faunal remains, glass, or metals. Based on the chronologies of the ceramic materials —giving particular importance to African Red Slip Ware (ARS), a tableware produced in north Africa that allows for a good dating precision—, the deposit has been dated to the first half of the 5th century but contained a few later materials from the end of the 6th century-early 7th century CE (Orfila and Cau, 1994; Cau, 2003; Buxeda Garrigós et al., 2005; and references therein). All samples ($n = 14$) can be considered on typological grounds typical of the first half of the 5th century (400–450 CE).

2.2. Es Castell (Ibiza)

The site of Es Castell (ESC) is a castle located in the uppermost part of the main town of Ibiza (Balearic Islands). Excavations in the castle allow for the definition of an interesting long stratigraphical sequence including evidence of late antique occupation of the area before the construction of the building. The 11 ceramic fragments studied belong to the C.205 stratigraphic level found on the northern side of tower II of the castle. The ceramic assemblage was composed of more than 300 vessels. These include some imported materials, consisting mainly of fine wares (African Red Slip wares and Gaulish 'dérivées-des-sigillées paléochrétiennes' or DS.P.), but also some cooking wares, a few amphorae, jars, and lamps. More than half of the assemblage corresponds to presumed local products (e.g., Ramon, 2008), including almost all the common wares, and very few amphorae (Ramon and Cau, 1997). This context has been dated after the ceramic study between 500 and 525 CE, with very coherent repertoire of ARS forms, and therefore corresponding to the Vandal period (455–534 CE) of the Balearics (Ramon and Cau, 1997).

2.3. Can Sorà (Ibiza)

The rural site of Can Sorà (CS) or Ses Païsses de Cala d'Hort is located in Sant Josep, in the western coast of Ibiza. It was a Punic rural settlement that developed into a Roman villa that was occupied also during Late Antiquity (e.g., Ramon, 1986, 1995). The 16 ceramics contained in this study were selected from different layers found in a cistern used as a rubbish dump in Late Antiquity. Four ceramic fragments were sampled from level II (575–625 CE), five from level IV (525–575 CE), and seven from level V (400–450 CE). The dating of the different contexts is based on the typological study of the ceramics with particular attention to the ARS forms (see for details, Ramon, 1994; Cau, 2003; Cau Ontiveros et al., 2019). The two first deposits from level II and IV represent the Byzantine period of the island, while level V is clearly pre-Vandal. Instead, the deposit from Es Castell is clearly dated in the Vandal period. Therefore, all the deposits selected from Ibiza cover a relatively precise sequence from 400– 450 to 575–625 CE covering the Late Roman, Vandal, and Byzantine periods of the island.

2.4. Early Christian church of Es Cap des Port de Fornells (Menorca)

The site is located at the bay of Fornells in northern Menorca (Balearic Islands). It includes and early Christian church, a baptistery, and a series of rooms forming a compact compound with a major occupation in Late Antiquity. This site of Fornells (F) has been interpreted as an ecclesiastical complex, probably a monastic community (de Palol, 1982; Gurt, 2007; Ripoll et al., 2012; Mas Florit et al., 2020). The materials analyzed ($n = 12$) are considered of local production —some of them imitating Galic manufactures known as Dérivées des Sigillées Paléochrétiennes (DS.P.)— and come from several assemblages recovered mainly in Rooms 39 (H.39) and 18 (H.18). The study of the archaeological materials suggests a dating between 500 and 550 CE for these deposits (Buxeda et al., Buxeda Garrigós et al., 1997).

2.5. Santhià

Near the small city of Santhià (SAN), in Vercelli Province, northern Italy (Fig. 1), at the location of Cascina Madonna (Strada Castelnuovo), a rescue archaeological excavation carried out in the occasion of the installation of a methane pipeline by SNAM Rete Gas Vercelli-Cavaglià, brought to light the remains of two rectangular brick kilns. Both kilns (kiln 7a and kiln 7b) are very similar in terms of type and materials; they are mainly made by fired clay, they have two parallel combustion chambers and their *praefurnii* are partially preserved. No chronological diagnostic artifacts were found in the site and the rescue nature of the excavation, with limited time and financial resources, has not permitted a precise dating of the structures based only on archaeological evidence. However, the type of kilns presents similarities to two other kilns excavated at Chieri (kilns B and C of the block of via della Gualderia-via Massa-via dei Giardini), whose activity is attested between the end of the 15th and the first half of the 16th century CE (Pantò and Vaschetti, 2010). A total of 22 in situ-oriented brick samples from the *praefurnium* of kiln 7a were collected and studied for combined archeomagnetic and thermoluminescence dating (Tema et al., 2019). The dating results obtained from these two different techniques are in excellent agreement, confirming that the last use of the kiln occurred around the 16th century CE. In this study, 12 fragments from the same bricks (Fig. 1), previously studied for archeodirection determination, were used here for archeointensity experiments. The dating of the bricks as determined through the thermoluminescence analysis is retained in this study, that is 1490–1574 CE (see details in Tema et al., 2019).

2.6. Velika

During the last decade, extended archaeological excavations in parallel with major public works, were carried out in Thessaly, Central Greece, between the city of Larissa and the Aegean coast. Late Antiquity phases of occupation are widespread in the area due to the fertile lands and the proximity of rivers and the sea. A thorough description of thirty such installations on the slopes of Mount Ossa is given by Sdrolia (2016 and references therein) and reveals a flourishing Late Antique phase with fortifications, rural villas, industrial areas, and a monastic

community. The whole network of installations is placed in the 6th century CE, that is Early Byzantine, with a reliable dating based on many findings among which pottery, glass and Emperor Justinian's coins found in the most important of the fortifications (Velika). In the present study we sampled another location, 5 kms to the south-east of Velika (Fig. 1), in the coastal settlement of Kato Sotiritsa where an orthogonal kiln of medium size (3 m x 3 m x 0.5 m) was excavated during the construction of a modern building (Fig. 1). We selected material from the kiln's walls (samples from 9 to 14) as well as large roof tiles from its production (samples from 1 to 4 and 6 to 7). The kiln, built on earlier soils, was dated in the 6th century CE upon the pottery found within its filling, identical to the one found and accompanied by Justinian's coins in other building plots of K. Sotiritsa and mostly in Velika Castle. Most of the fortresses in the area were abandoned during the 7th century CE when inhabitants moved away from the sea (Sdrolia, 2016).

3. Methodology

3.1. Rock-magnetism experiments

Rock magnetic studies were carried out on sub-samples prepared from fragments or block off-cuts at the paleomagnetic laboratory of the Complutense University (Madrid). These experiments were performed in several samples per site in order to identify the main magnetic minerals carrying the thermoremanence of the samples as well as to evaluate their thermal stability. The laboratory procedures followed are similar to those described in detail in Rivero-Montero et al. (2021). Rock-magnetic experiments include low-field magnetic susceptibility measurements, magnetic hysteresis and back-field isothermal remanence (IRM) curves, thermomagnetic curves, IRM acquisition curves, thermal demagnetization of orthogonal IRMs and First-Order Reversal Curves. Low field magnetic susceptibility was measured using a KLY-4S kappa-bridge (AGICO). Hysteresis loops, IRM acquisition and back-field IRM, were measured on crushed samples using a coercitivity spectrometer developed in the University of Kazan (Jasonov et al., 1998) with a maximum applied field of 500 mT. The saturation of magnetization (Ms), the remanent magnetization after saturation (Mr) and the magnetic coercivity (Hc) were determined after eliminating the paramagnetic contribution (Butler, 1998). The coercivity of remanence (Hcr) was estimated from back-field IRM curves. The contribution of superparamagnetic grains to the remanent magnetization was calculated from the decay between the IRMs measured just after applying 500 and 0 mT (see Enkin et al., 2007). The thermomagnetic curves (K-T curves) were measured with a KLY-4S equipped with a high-temperature furnace apparatus (AGICO). The K-T curves were performed in Ar atmosphere, warming up to around 650 °C and then cooling down to 40 °C. The thermal demagnetization of orthogonal IRM cross components were made following the protocol proposed by Lowrie (1990). Orthogonal IRMs were applied to the samples using an ASC Scientific IM-10-30 impulse magnetizer applying magnetic fields of 2 T, 0.4 T and 0.12 T along three orthogonal axes. Samples were thermally demagnetized in a Schonstedt thermal demagnetizer manufactured by Magnetic Measurements, and magnetization measurements were made using a Minispin (Molspin) spinner magnetometer. In addition, the thermal demagnetization of orthogonal IRMs experiments from four Santhià samples were performed at the CIMaN-ALP Alpine paleomagnetic laboratory (Italy) following the same protocol. Finally, eight First Order Reversal Curve (FORC) experiments were carried out on selected potteries (2 per site) at the Institut de Physique du Globe de Paris (Paris) with a vibrating sample magnetometer (μ-VSM) from Princeton Measurements Corporation. The FORC diagrams were measured with an averaging time of 100 ms and with a saturating field of 1.5 T and 250 FORCs by FORC diagram. To analyze the FORC diagrams, we used the VARIFORC software of Egli (2013).

3.2. Archeointensity determination

The experimental procedures followed are similar to those applied in our recent study (Rivero-Montero et al., 2021). Between one and four specimens per sample (103 in total) were prepared at the paleomagnetic laboratory of the Complutense University of Madrid. For the pottery fragments, specimens of about 1.5×1.5 cm^2 were prepared and packed into quartz cubes using fiberglass and waterglass. For Velika and Santhià, cylinders of about 2 cm of diameter and 2 cm-long were prepared. For archeointensity determination, we followed the Thellier classical method (Thellier and Thellier, 1959) including partial thermoremanent magnetization (pTRM) checks, TRM anisotropy and cooling rate corrections. Between 10 and 14 temperature steps (from 100 to 600 °C) were performed. Specimens were heated during 45 min using Magnetic Measurements Thermal Demagnetizer ovens MMTD80 or MMTD24. At each temperature step, the specimens were heated and cooled applying a field of 50 μT, first with the field applied along their z-axis (defined as the long and short axes for the standard cylinders and the potteries, respectively) and then with the field applied in the opposite sense. The magnetic remanences of the potteries were measured with a superconducting rock magnetometer (2G). For the other samples, we used a Minispin (Molspin) spinner magnetometer. Experiments also included low-field bulk susceptibility measurements performed with a Bartington MS3 susceptibility meter after each temperature step and partial thermoremanent magnetization (pTRM) checks every two temperature steps. Both measurements allow checking for possible magnetic alteration during heating. TRM anisotropy tensors were measured when around 70% of the initial Natural Remanent Magnetization (NRM) was lost. For this purpose, six additional steps were measured with the magnetic field applied along six orthogonal axes (+x, −x, +y, −y and +z, −z). The last +z step was used to check for possible thermally-induced alteration during the TRM anisotropy protocol. All the archeointensity measurements were corrected according to the obtained ATRM tensor. The cooling rate dependence of TRM intensity was also analyzed by measuring four additional TRM acquisition steps after the end of Thellier experiments. Comparing the rapid (the typical laboratory cooling time of about 1.5 h) and slow cooling results (of about 24 h) we quantified the cooling rate effect upon archeointensity estimates for each specimen. This protocol also includes the determination of an alteration factor used to estimate changes in the TRM acquisition capacity of the specimens during the cooling rate protocol. We used a slow cooling time of about 24 h but no robust information about the real past cooling time followed by our samples is available. However, we note here that a recent publication suggests that incorrectly estimating the duration of the ancient archaeological cooling has a limited impact on the accuracy of the archeointensity data at least in the archaeological fired clays studied by the authors (Hervé et al., 2019). The results of this publication emphasize the necessity of cooling rate correction but also indicate that different tested cooling rates (between 10 and 76 h) give average intensities close to the expected value (see Hervé et al., 2019 for details). For a more detailed description of the experimental procedures followed for the TRM anisotropy and cooling rate corrections, see Gómez-Paccard et al. (2006). The treatment of the data was performed with the StarmacAWE2.0 software developed by Pierrick Roperch at Univ Rennes, CNRS, Géosciences Rennes, UMR 6118.

The establishment of robust and objective criteria to select the most reliable intensity estimations is not an easy task and has been largely discussed in the literature (e.g., Chauvin et al., 2000; Genevey et al., 2008; Paterson et al., 2014). Here, we applied several quality criteria at the specimen level following our previous studies (Gómez-Paccard et al., 2006, 2019; Rivero-Montero et al., 2021). Archeointensity estimates were only determined from well-defined single components of magnetization pointing to the origin in the Zijderveld plots. At least five temperature steps must be selected for archeointensity determination. Only estimations related to maximum angular deviation (MAD; Kirschvink,

1980) and deviation angles (DANG; Pick and Tauxe, 1993) lower than 5° were retained. We also checked the fraction of the remanence used for calculation of the intensity values as well as the scatter, linearity, and alteration effects in the NRM–TRM plots. The f parameter (NRM fraction, Coe et al., 1978) must be at least 50%. The ratio of the standard error of the slope to the absolute value of the slope (β) must be lower than 0.1 (Shaar et al., 2016). NRM–TRM diagrams must be linear and pTRM checks, including the alteration checks made after the determination of the ATRM tensors and cooling rate factors, lower than 10% of the total TRM acquired.

Finally, we calculated a mean value per archaeological group by averaging the intensities obtained at the specimen level, defining an archaeological group as the ceramics of the same archaeological layer, the hand samples from the same kiln (SAN and VE) and the group of tiles from VE. The samples from the walls of the kiln VE and the tiles from its production were treated as separated groups as there is no robust archaeological evidence that they correspond to the same heating event since the tiles were found piled outside but close to the kiln. Only the mean values derived from at least three different specimens were retained.

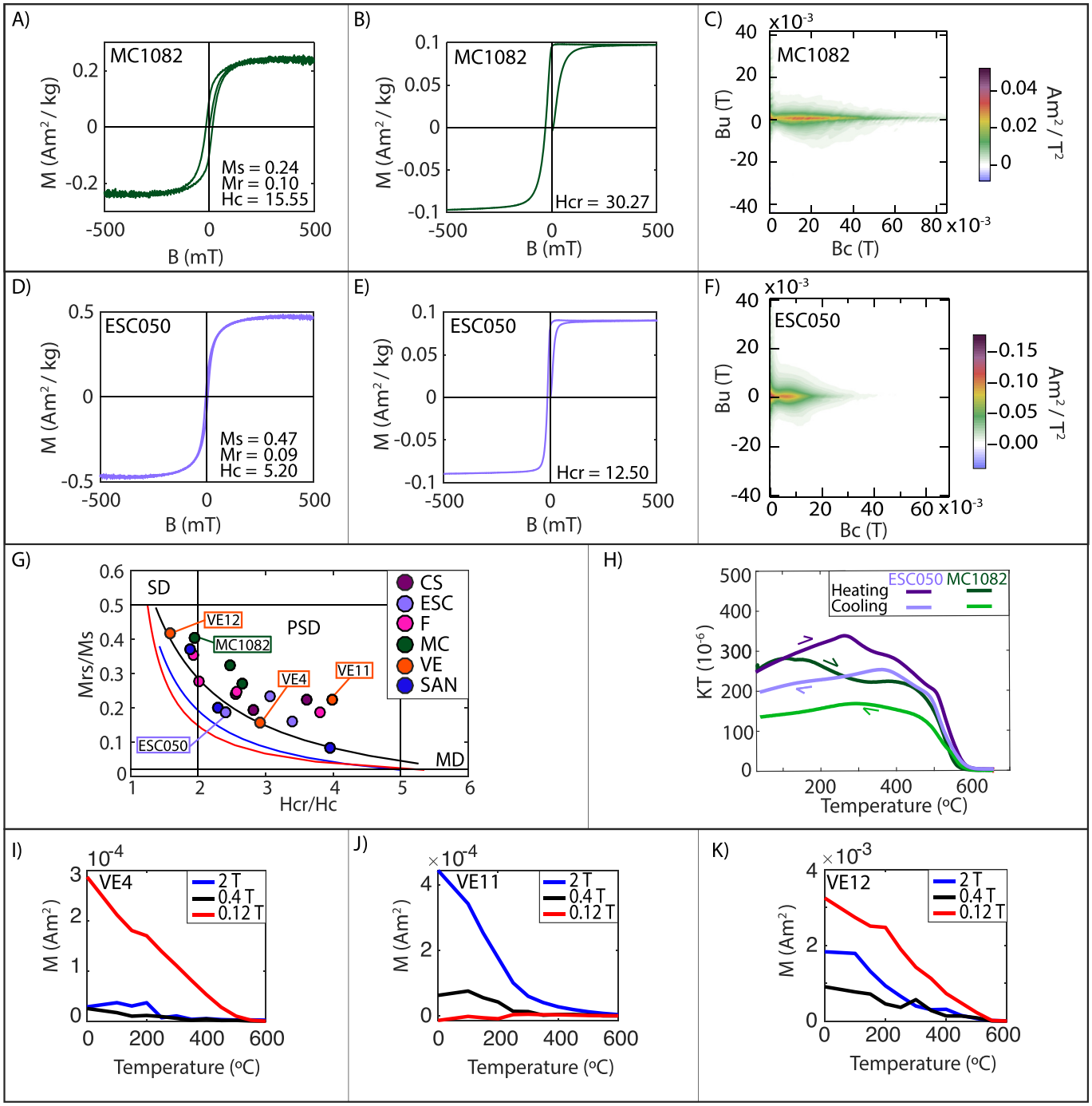

Fig. 2. Rock magnetic results. A) and D) Hysteresis loops measured up to 500 mT and corrected for the paramagnetic contribution. B) and E) SIRM (saturation isothermal remanent magnetization) and back field SIRM curves. C) and F) First-Order Reversal Curves (FORCs). G) Day plot (Day et al., 1977) with SD (single domain) – MD (multidomain) mixing curves for magnetite (Dunlop, 2002). H) Thermomagnetic K-T curves. I), J) and K) Thermal demagnetization of orthogonal IRMs (Lowrie, 1990).

4. Results

4.1. Rock magnetism

Initial Natural Remanent Magnetization (NRM) intensities vary between $2.0{\cdot}10^{-4}$ and $2.5{\cdot}10^{-2}$ Am^2/kg. 25 hysteresis loops with IRM acquisition and back-field IRM were measured. Several samples per site were analyzed. Magnetic hysteresis cycles are closed with non-constricted loops that saturate at about 150–300 mT and with coercivities in the range of 4 and 16 mT (Fig. 2A and D) suggesting the dominance of low coercivity minerals. Isothermal remanent magnetization (IRM) acquisition experiments up to 500 mT show that most of the samples saturate between 150 and 300 mT (Fig. 2B and E). However, a few samples from Velika do not completely saturate at the maximum applied field of 500 mT. Reversal of IRM acquisitions show a decrease of the remanence when switching the field, indicating a significant superparamagnetic (SP) fraction (Fig. 2E). IRMs up to 2 T and further thermal demagnetization of IRM-cross components (Lowrie, 1990) performed on 13 samples from VE and SAN confirm the presence of a low coercivity phase such as magnetite/titanomagnetite in the samples of these sites (Fig. 2I and K). Some samples also display the presence of a higher coercivity phase such as hematite or epsilon hematite (Fig. 2I and J).

The magnetic hysteresis-derived parameters from the saturated samples from all the sites were plotted on the Day-Dunlop plot (Dunlop, 2002). All the studied samples fall into the single domain (SD) and pseudo-single domain (PSD) regions of the Day-Dunlop plot (Fig. 2G). However, some samples deviate from the general behavior and are shifted to the right or up, very likely due to the presence of SD and/or high coercivity minor traces. This is in agreement with the eight FORCs diagrams obtained, where we can see the presence of two peaks: one very close to the origin with vertical contours characteristic of SP grains, and one centered at coercivities of around 4–16 mT, that might be attributed to stable SD grains (Roberts et al., 2000), as seen in Fig. 2C and F.

Nine K-T curves were measured including samples from the Spanish and Greek archaeological sites. Curie temperatures range between 530 and 580 °C and the shape of the K-T curves suggest the presence of magnetite/titanomagnetite with variable Ti content. In some curves, the samples show a small increase in the susceptibility in the range of 300–350 °C, suggesting the presence of maghemite (Fig. 2H) (Kontny and Grothaus, 2017).

Altogether the rock-magnetic results suggest that the main magnetic carrier observed in the Spanish pottery fragments is magnetite and titanomagnetite, sometime with low maghemite contribution, with a very homogenous behavior within samples from the same site. For Santhià kiln, in the samples for which rock-magnetic experiments are available, a similar magnetic behavior characterized by low coercivity minerals is observed. In Velika two different kind of samples were studied: fired clays taken from the walls and a collection of tiles. In the fired clays from the walls the magnetization is mainly controlled by magnetite and titanomagnetite. In the tiles, in addition to these two minerals, epsilon hematite is also seen in the thermal demagnetization of IRM cross components. A deeper analysis of the IRM acquisition curves by means of coercivity spectral analysis at VE site reveals that differences in magnetic mineralogy are related to the archeo-lithology not the location of the samples.

Magnetite/titanomagnetite (Fig. 2I, K and G), hematite (Fig. 2I), maghemite (Fig. 2H) and epsilon hematite (Fig. 2I and K) seem to be the four actors present in the samples, although concentration is highly variable. However, recent studies have shown that local conditions are key to develop magnetic mineralogy at sub-centimetric scale (López-Sánchez et al., 2020). The overall result of the rock magnetic experiment (and Thellier experiments as we will explain in the next section) summarizes how the magnetic signal is dominated by SD or mainly SD particles. Most samples studied of the different sites suggest the presence of magnetite and/or titanomagnetite with variable Ti-content.

4.2. New archeointensities

The 63.2% of the studied specimens passed the selection criteria applied at the specimen level and resulted into linear NRM-TRM diagrams corresponding to a single component of magnetization going towards the origin in the Zijderveld plots that is well isolated, after a small viscous component, between 100–200 °C and 440–560 °C (Fig. 3A). The linearity of the selected NRM/TRM with no evidence of concave up behavior, together with the rock-magnetic results described above, suggests the dominance of SD magnetic grains in the selected samples. In the other cases, a more complex behavior was observed, with several components of magnetization, concave up pattern or evidence of important mineralogical changes during Thellier experiments (Fig. 3B). Such specimens were rejected fromarcheointensity determination.

Successful results are summarized in Table S1 of the Supplementary Material. The success rates associated with the archeointensity study are higher for the Spanish potteries with rates ranging between 75% and 100% for the different studied groups (see Table 1). For Velika, the success rate is low, with only about 20% retained specimens for the tiles and 47% for the kiln samples. In the case of Santhià, about 44% of the specimens studied passed the selection criteria. The differences observed between the high success rates for potteries and the low rates obtained for the kilns and tiles could be explained by the fact that the Spanish potteries are more fine-grained than the other samples. Moreover, in some cases important mineralogical alterations were observed in the kiln's samples and, hence, the corresponding f factors were lower than 0.5 and the specimens were discarded. The NRM fractions used for archeointensity determination (f parameter) range between 0.53 and 0.98 and quality factors (q) between 7.2 and 79.7, all of them corresponding to MAD and DANG angles lower or equal to 5° (Fig. 4 and Table S1).

The effect of the TRM anisotropy upon archeointensity estimates has been corrected at the specimen level. The differences between the corrected and uncorrected intensities are plotted in Fig. 4C. As expected, the TRM anisotropy effect is higher for the potteries and tiles than for the fired clay fragments from the kilns for which very similar intensity values are generally obtained before and after the TRM anisotropy correction (see Fig. 4C). The cooling rate (CR) effect has also been investigated in all the specimens. The mean CR correction value for our collection is 7.6%, with the highest values obtained for the VE tiles (up to 18%) (Fig. 4F). When it was not possible to experimentally determine the CR due to evidence of mineralogical alteration at high temperatures, we applied a mean value derived from the CR effect measured for the other specimens of the same group or, if this was not possible, we applied a 5% CR factor as suggested for older studies (Genevey et al., 2008) and in agreement with other results performed on archaeological fired clays (e.g., Hervé et al., 2019).

From the results accepted at the specimen level, we calculated a mean intensity per group (see Table 1). Only mean intensities derived from at least three different specimens were retained. In general, we found very similar intensities between specimens from the same group. The standard deviation/mean intensity ratios (σ_m/Fm in Table 1) are lower than 10% for all the groups except for the tiles of Velika. Mean intensities range between 51.7 ± 4.5 and 68.0 ± 1.1 μT corresponding to Virtual Axial Dipole Moment (VADM) values between 89.9 ± 7.8 and 119.0 ± 1.9 ZAm^2, respectively. The new data obtained from the Balearic Islands (Spain) support the presence of a rapid intensity increase between 400 and 625 CE corresponding to the initial phase of the double-oscillation in Western Europe (see Fig. 5A). The results obtained from the tiles and wall's fragments from the kiln sampled at Velika (Greece) indicate that the geomagnetic field intensity was of about 60–62 μT during the 6th century CE in the region. Moreover, the values obtained are similar to the one obtained from a collection sampled in the same area and of the same period (TEM kiln from Tema et al., 2012). The

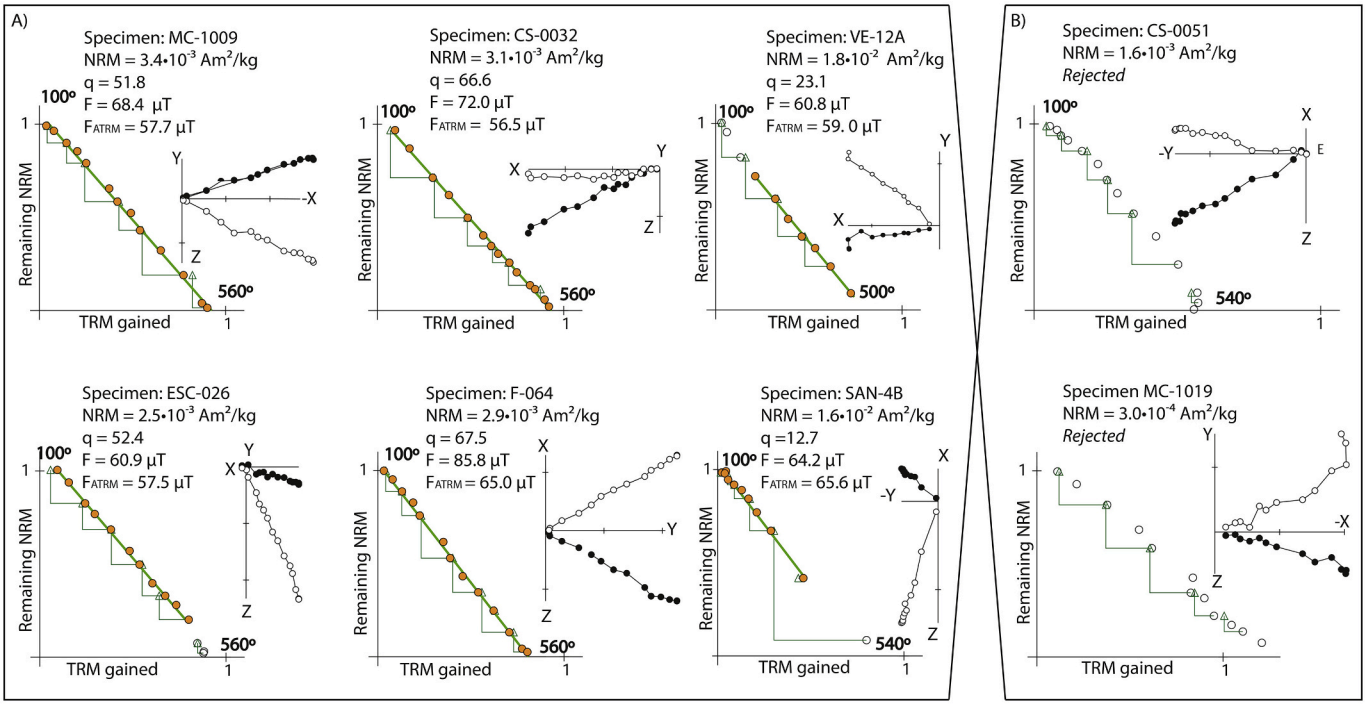

Fig. 3. A) NRM (natural remanent magnetization) - TRM (thermoremanent magnetization) diagrams for representative specimens together with the corresponding Zijderveld plots. Orange points and green lines correspond to the temperature interval selected for archeointensity determination. The initial natural remanent magnetization (NRM), the quality factor q (Coe et al., 1978) and the archeointensity obtained before (F) and after (F_{ATRM}) the anisotropy corrections are indicated. B) Examples representative of rejected specimens. (For interpretation of the references to colour in this figure legend, the reader is referred to the web version of this article.)

Table 1
Summary of the new archeointensities obtained for Europe. Country, country of origin; Site, name of the archaeological site; Lat. and Long., geographical coordinates. Material and Lab code, Material and Laboratory code for the studied collection; Date, indicate the age ascribed to each group; N_S (n_S), number of samples (specimens) studied in the laboratory; N_R (n_R), number of samples (specimens) retained to calculate mean intensities; F ± σ, mean intensity and standard deviation before corrections; $F_{ATRM} \pm \sigma_{ATRM}$, mean intensity and standard deviation corrected for the TRM anisotropy effect; $F_m \pm \sigma_m$, mean intensity and standard deviation corrected for the TRM anisotropy and cooling rate effects upon archeointensity estimates; σ_m/Fm, standard error/mean intensity; VADM, values of the virtual axial dipole moment ± error.

Country	Site *(Lat. Long.)*	Material	Lab. Code	Date (yrs CE)	N_S	N_R	n_S	n_R	F ± σ (μT)	$F_{ATRM} \pm \sigma_{ATRM}$ (μT)	$F_m \pm \sigma_m$ (μT)	σ_m/ Fm (%)	VADM (ZAm^2)
Spain	Sa Mesquida	Pottery	MC	400–450 CE	14	11	14	11	62.9 ± 11.1	56.6 ± 5.3	51.7 ± 4.5	8.8	89.9 ± 7.8
	(39.52°N, 2.49°E)												
	Es Castell	Pottery	ESC	500–525 CE	11	10	11	10	69.7 ± 6.3	61.5 ± 4.5	56.7 ± 4.8	8.4	99.2 ± 8.4
	(38.91°*N*, 1.42°*E)*												
	Can Sorà	Pottery	CS - Nivel V	400–450 CE	7	7	7	7	68.0 ± 6.9	59.3 ± 3.8	55.2 ± 3.1	5.6	96.6 ± 5.4
	(38.89°*N*, 1.22°*E)*	Pottery	CS - Nivel IV	525–575 CE	5	4	5	4	87.3 ± 4.1	73.2 ± 0.6	68.0 ± 1.1	1.6	119.0 ± 1.9
		Pottery	CS - Nivel II	575–625 CE	4	3	4	3	78.4 ± 15.5	67.6 ± 5.0	61.9 ± 5.9	9.5	108.4 ± 10.3
	Fornells	Pottery	H.39	500–550 CE	5	4	5	4	69.7 ± 12.8	59.7 ± 6.1	55.5 ± 3.4	6.1	95.8 ± 5.9
	(40.06°*N*, 4.13°*E)*	Pottery	H.18	500–550 CE	7	7	7	7	70.5 ± 7.9	60.3 ± 5.8	57.6 ± 5.3	9.1	99.4 ± 9.1
Italy	Santhià	Kiln	SAN	1490–1574 CE	12	5	18	8	61.4 ± 4.0	61.6 ± 3.1	59.2 ± 3.0	5.1	96.4 ± 4.9
	(45.37°N, 8.17°E)												
Greece	Velika	Tiles	VE Tiles	500–600 CE	6	2	15	3	93.4 ± 19.4	73.6 ± 6.6	62.7 ± 7.4	11.9	108.7 ± 12.8
	(39.73°N, 22.85°E)	Kiln	VE Kiln	500–600 CE	6	4	17	8	65.2 ± 6.0	64.0 ± 5.0	60.7 ± 4.7	7.7	105.3 ± 8.2

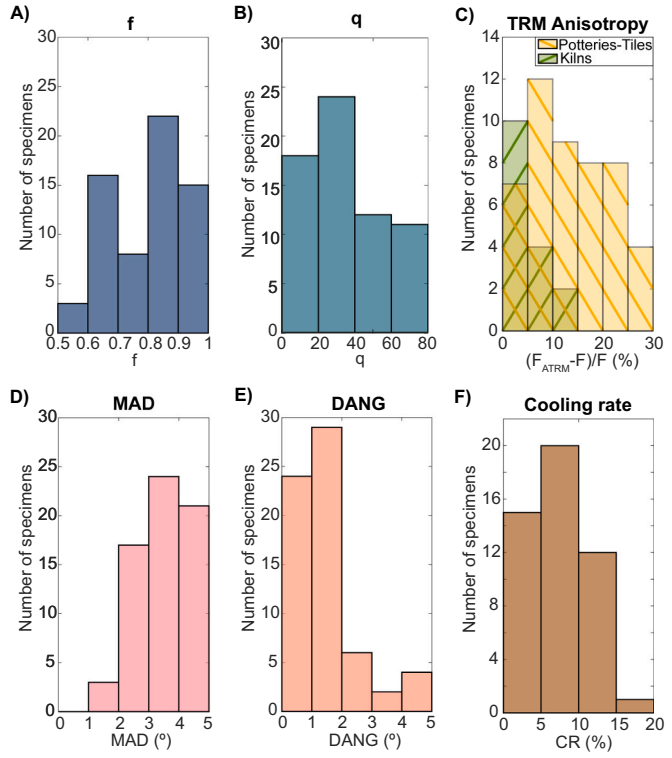

Fig. 4. Quality parameters and TRM anisotropy and cooling rate (CR) correction factors of retained specimens (Table S1). A) f, fraction of the NRM. B) q, quality factor. C) TRM anisotropy correction factor. D) MAD, maximum angle of deviation. E) DANG, deviation angle. F) CR, cooling rate correction factor experimentally determined in this study.

new Greek data also allow to better constrain the geomagnetic field strength during the initial increase phase of the double-oscillation (Fig. 5B). Finally, a mean value of 59.2 ± 3.0 μT was obtained for Santhià (Italy), giving additional information to better define the relative maximum achieved at the beginning of the 15th century CE in Western Europe (Fig. 5A). For the Santhià kiln, an archeomagnetic direction obtained in a previous publication was already available so the new data offer a full geomagnetic field vector record for the beginning of the 15th century CE in Italy (Tema et al., 2019).

5. Discussion

In order to refine the past changes of the geomagnetic field strength in Europe between 200 CE and 1800 CE, we compiled the European archeointensities using the GEOMAGIA50v3.4 database updated in January 2021 (Brown et al., 2015). One of the main problems involved in geomagnetic field intensity reconstructions is the quality assessment of the input data used for modeling the field. It has been largely recognized that some of the older studies contain some archeointensities that might not be accurate markers of past geomagnetic field strength (e.g., Chauvin et al., 2000; Genevey et al., 2008). Here and following our previous studies (Gómez-Paccard et al., 2012; Campuzano et al., 2019; Pavón-Carrasco et al., 2021) we selected data following different quality criteria based on the type of material analyzed, the number of specimens retained to calculate the mean values and the laboratory protocol followed to obtain the archeointensities. We selected data obtained from three or more specimens and derived from Thellier type methods including partial pTRM checks. For ceramics or highly anisotropic materials, only data considering the correction of the TRM anisotropy effect upon intensity estimates were selected. Following the results of Genevey et al. (2008) for older studies, a 5% decrease of the intensity values was applied when the cooling rate correction factor was not experimentally determined. Finally, it is important to note that a specific criterion regarding the uncertainties around the mean intensity values has not been applied. After this selection, we compiled the data corresponding to an area of 7° of radius (~780 km) centered in two locations: 45°N / 5°E (France) for Western Europe and 45°N / 25°E (Romania) for Eastern Europe (see dark blue and orange circles in Fig. 6). From 200 CE to 1800 CE, 138 data from Western Europe (Hedley and Wagner, 1991; Chauvin et al., 2000; Genevey and Gallet, 2002; Gómez-Paccard et al., 2006, 2008, 2012; Spassov et al., 2008; Gallet et al., 2009; Genevey et al., 2009, 2013, 2016, 2019; Kovacheva et al., 2009; Tema et al., 2010, 2015; Donadini et al., 2012; Schnepp and Brüggler, 2016; Schnepp et al., 2020) and 77 from Eastern Europe (Burlatskaya, 1970; Burlatskaya et al., 1986; Ogishima et al., 2000; De Marco et al., 2008; Kovacheva et al., 2009, 2014; Spatharas et al., 2011; Tema et al., 2012; Kondopoulou et al., 2015; Aidona et al., 2018; Genevey et al., 2018; Schnepp et al., 2020) pass our selection criteria (Table S2). As it can be seen in Fig. 5A and B, our new archeointensities are in agreement with the selected data, both in Western and Eastern Europe. Only the new intensity obtained for the CS-Nivel II group (575–625 CE) seems to be outside the general trend given by the previous coetaneous data (Fig. 5A). This datum presents a large standard deviation (5.9 μT) due to the discrepancy between the three intensities derived at the fragment level. The datum passes the quality criteria used in this work and thus no scientific reason can be considered to discard it from our analysis. However, this scatter could also be explained by a strong variation of the geomagnetic field strength over the time interval associated to the context (50 years) and therefore the fragment CS0062 (fragment recording the lowest intensity for the CS-Nivel II group) could be older than the rest of fragments of the same group.

From the compiled datasets (Table S2) and the new data presented here, we calculated two new intensity PSV curves for Western (45° N, 5° E; France) and Eastern Europe (45° N, 25° E; Romania) (Table S3). The curves were developed following the method proposed by Thébault and Gallet (2010). A time fitting was applied using temporal cubic b-splines by means of a bootstrap approach that considers both age and intensity uncertainties. In contrast to Thébault and Gallet (2010), our modeling approach does not reweight the archeointensity data by the residuals. The bootstrap provides an ensemble of 5000 PSV curves whose mean and standard deviations can be estimated providing a single continuous PSV curve with its error bar at 68 or 95% of probability (see Rivero-Montero et al., 2021 for details). The two PSV curves clearly show a sequence of intensity maxima between 200 and 1800 CE (Fig. 5). From a first visual inspection, it seems that the observed maxima were achieved at different times in Western and Eastern Europe. According to the Western Europe PSV curve (Fig. 5A), the maxima occurred around 310 CE, 620 CE and 820 CE (corresponding to the double-oscillation), 1140 CE, 1380 CE and 1600 CE; with maximum values of 63.0 ± 5.1 μT, 76.5 ± 4.9 μT, 76.9 ± 3.5 μT, 59.3 ± 3.7 μT, 55.7 ± 3.0 μT and 54.1 ± 2.5 μT, respectively (errors at 95% of probability). Whereas in Eastern Europe (Fig. 5B), the maxima are identified at 350 CE, 670 CE and 940 CE (the double-oscillation), 1300 CE, 1580 CE and 1710 with intensities of 59.0 ± 6.3 μT, 72.2 ± 14.4 μT, 74.6 ± 8.0 μT, 56.8 ± 4.1 μT, 61.2 ± 7.3 μT and 56.6 ± 5.9 μT, respectively (errors at 95% of probability). It is important to note that, however, some of these maxima are not well defined such as the 310 CE maximum for Western Europe or the 350 CE maximum for Eastern Europe and, hence, more data are needed in order to robustly define them. In spite of some uncertainties of the maxima depicted the trend of the obtained curves suggests, however, that the Eastern maxima seem to occur several decades later than those observed in Western Europe. However, considering the uncertainties associated with the PSV curves and represented by the error bands at 95% of probability, this result should be considered with caution. To deeply investigate the potential lag-time between the curves, we perform an additional statistical study that is explained in detail at the end of this section.

The new PSV curves are then compared with previous PSV curves

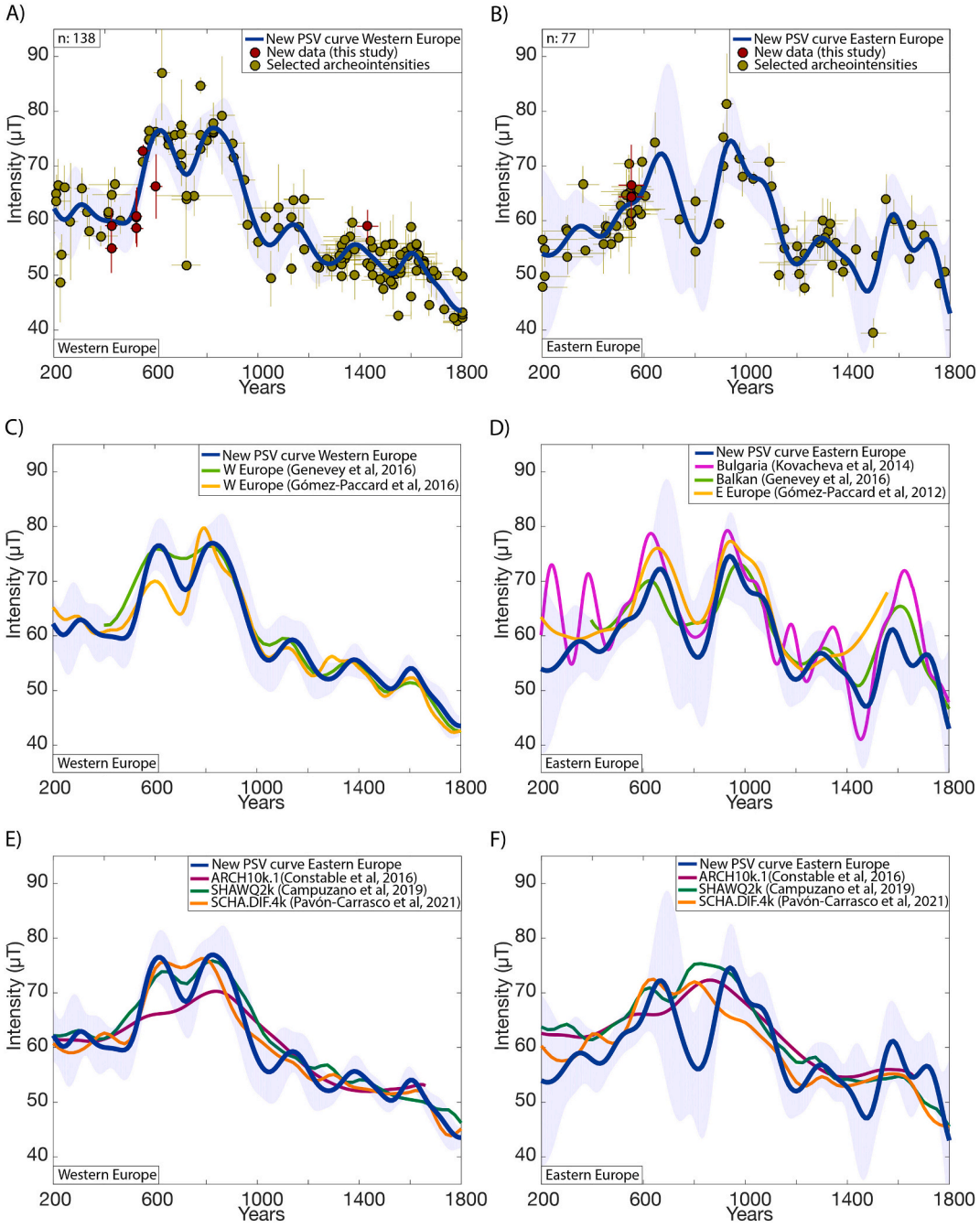

Fig. 5. New PSV curves (blue lines) obtained for Western and Eastern Europe plotted with its 2-sigma error band (shaded areas) and compared to: A) and B) New archeointensity results (red circles) obtained in this study and previous selected results (green circles). **n**: is the number of data represented at each figure and used to calculate the new PSV curves. C) and D) PSV regional curves from previous studies. E) and F) Different regional and global models results. Data, curves, and models are all relocated to 45° N, 5° E for Western Europe and 45° N, 25° E for Eastern Europe. (For interpretation of the references to colour in this figure legend, the reader is referred to the web version of this article.)

(see Fig. 5C and D) and with the predictions derived from different regional and global archeomagnetic models (see Fig. 5E and F). In Western Europe (Fig. 5C), the double-oscillation feature (with two maxima around 620 CE and 820 CE in our curve) was already recorded in previous curves but showing a smoother behavior (Genevey et al., 2016) or lower intensity values for the first maximum and higher for the second (Gómez-Paccard et al., 2016) than those provided by our new PSV curve. Thanks to the new data obtained here the starting point of the first bump of the double-oscillation feature is now better defined. It is worth noting than the pronounced minimum observed now between the two maxima of the double-oscillation (around 720 CE) is linked to new intensity data acquired recently by Schnepp et al. (2020) and thus not available when the previous curves were constructed. Finally, a satisfactory agreement is found between the previous curves and the new obtained here for the last maxima (1140 CE, 1380 CE and 1600 CE), highlighting that even if the selected input data and regions used in the different publications are not exactly the same, the observed trend of oscillations seems to be well constrained in Western Europe (except the small maximum around 310 CE that needs to be further studied). When compared to the most recent regional and global archeomagnetic models (Fig. 5E) it can be seen how the models show a clear smoother behavior during the whole period. Although the SHAWQ2k (Campuzano et al.,

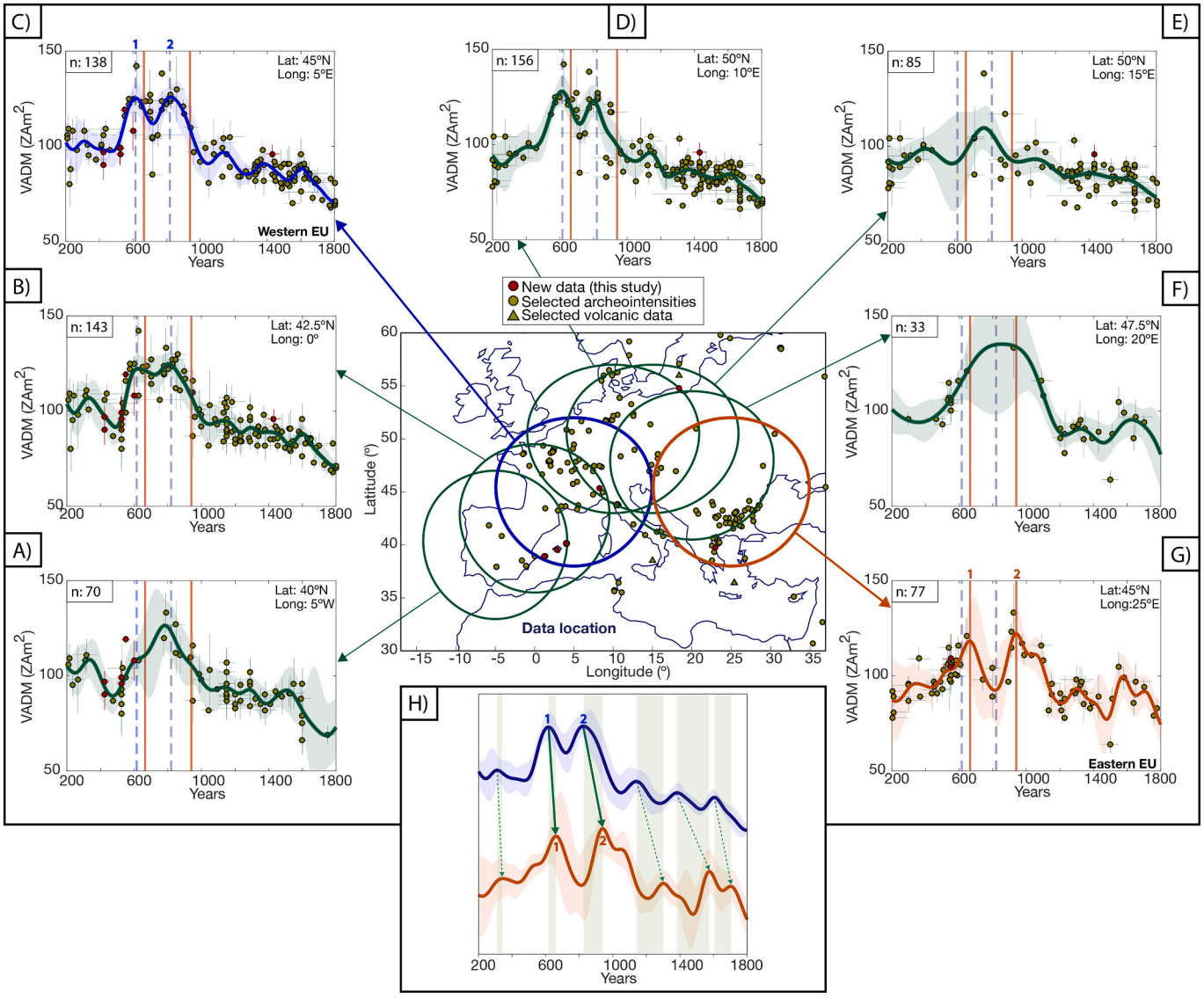

Fig. 6. A-G) PSV intensity curves between 200 CE and 1800 CE calculated for different regions, being the regions represented by circles in the central map. **n**: is the number of data represented at each figure and used to calculate the corresponding PSV curve. The shaded areas represent the 2-sigma error band of the curves. The new data obtained here are shown in red circles and previous data from other studies in green. The dashed lines correspond to the maxima in Western Europe (620 CE and 820 CE) and the continuous lines correspond to the maxima in Eastern Europe (660 and 940 CE). H) Possible correlation between the maxima identified in the Western Europe (in blue) and Easter Europe (in orange) curves. The shaded areas show the temporary differences between the maxima deduced from the correlation proposed. (For interpretation of the references to colour in this figure legend, the reader is referred to the web version of this article.)

2019) and SCHA.DIF.4 k (Pavón-Carrasco et al., 2021) models show the double-oscillation feature, they do not capture the occurrence of intensity maxima after the double-oscillation. This highlights the necessity to implement robust local PSV curves, since they are the best approach to accurately determine the past variations of the geomagnetic field at regional scales. For the ARCH10k.1 model (Constable et al., 2016) the smooth behavior is more noticeable and the double-oscillation feature is not observed. Differences between the model predictions can also be related to the used input data, since the SHAWQ2k and SCHA.DIF.4 k models applied similar selection criteria than those used in this study, while the ARCH10k.1 model used all the available data regardless of the laboratory methodology used to obtain them.

In Eastern Europe (Fig. 5D), the previous PSV curves and the new one show different behaviors although the general trend is quite similar. The Bulgarian curve published in 2014 (Kovacheva et al., 2014) showed a trend of oscillations, including the double-oscillation feature, with significant amplitudes (corresponding to rates of change up to 21.5 μT/century). Since neither our selected high-quality dataset nor the new PSV curve present this high variability, we suggest that some of the Bulgarian maxima and minima are controlled by some archeointensities that do not accomplish modern standards of quality. In fact, some of these oscillations are described by archeointensities derived from the Thellier method but not including pTRM cheks so not included in our dataset. Our new curve clearly fits better the Genevey et al. (2016) and Gómez-Paccard et al. (2012) curves, which show several maxima, including the double-oscillation event. It is important to note that, according to all the PSV curves, the double-oscillation shows a stronger decline in intensity between the two peaks in Eastern (with a minimum of 56.1 μT in our curve) than in Western Europe (with a relative minimum of 68.4 μT in our curve). The minimum in Eastern Europe is controlled by four low and quite consistent intensity values (Kovacheva et al., 2014; Spatharas et al., 2011). In Western Europe, although 16 data are available (Genevey et al., 2016; Gómez-Paccard et al., 2012; Kovacheva et al., 2009; Tema et al., 2010; Schnepp et al., 2020), only four of

them suggest a more pronounced minimum as mentioned above (Gómez-Paccard et al., 2012; Schnepp et al., 2020). More well dated archeointensities, both for Eastern and Western Europe are needed to further discern this issue. As for Western Europe, the regional and global models show again smoother trends for the intensity element at these regional scales (Fig. 5F).

Since the double-oscillation event is the most important feature of the European geomagnetic field strength over the last two millennia, we tried to evaluate the time and spatial evolution of this event throughout Europe. To do that, we obtained the PSV curves for five additional regions (all of them with 7° of radius) in Europe following the same methodology explained before (see map in Fig. 6). Despite the great effort made during the last years, the number of archeointensity data is still very low for some of the selected regions. For example, in Iberia (Fig. 6A) the lack of data between 600 and 800 CE has not allowed to identify the minimum between the two maxima of the double-oscillation and, hence, a single maximum is seen in the PSV curve. In central Europe, the PSV curves of the regions "50°N / 15°E" (Fig. 6E) and "47.5°N / 20°E" (Fig. 6F) are not well defined between 500 and 700 CE and 700 and 850 CE, respectively, due to the low number of data available. More data are clearly needed in order to better define geomagnetic field intensity changes all over Europe during this period.

Despite these gaps, the differences of the oscillation intensity trends observed between the Western and Eastern Europe can be analyzed. As indicated before, a visual inspection of the results obtained for the double-oscillation event suggests that there is a time delay between the maxima observed in Western Europe and those recorded in the Eastern side of this continent (Fig. 6H). However, considering the uncertainties associated with the PSV curves and represented by the error bands at 95% of probability, this hypothesis should be considered with caution. An interesting study in terms of frequency and correlation between the observed oscillation trends can be attempted. To quantify the visual correlation proposed in Fig. 6H, we carry out two more sophisticated studies using the Western and Eastern European curves.

The first study is focused on the estimation of the characteristic periods found in both curves. To do that, we use two different approaches: the empirical mode decomposition (EMD, Flandrin, 2009) and the wavelet analysis. The EMD method provides the characteristic period considering the error bars of the curves by means of a Monte-Carlo bootstrap, and transferring the intensity error to the uncertainty of the characteristic periods. Results are given in Fig. 7A. It can be seen that the Western curve is characterized by a period of about 275 ± 20 yr, this result being consistent with the period proposed by Genevey et al. (2016) (~250 yr) and Livermore et al. (2018) (269 ± 9 yr) for Western Europe for the last 1500 yr. The Eastern curve presents a higher period of about 325 ± 30 yr, corresponding to the average dominant period for the whole-time interval in statistical terms, although it may be not representative for last two maxima separated just by 130 yr. The Western and Eastern periods are indistinguishable in the range between 250–350 yr (overlapping window of the histograms).

The wavelet analysis allows to know how the characteristic periods of the curves are distributed within the considered time window, i.e. 200 CE – 1800 CE. For each PSV curve, the wavelet analysis is shown in Fig. 1S (left panel). For the Western curve, the wavelet shows a clear period of about 270 yr (in agreement with the EMD study) for the whole time window. However, the wavelet of the Eastern curve shows a large

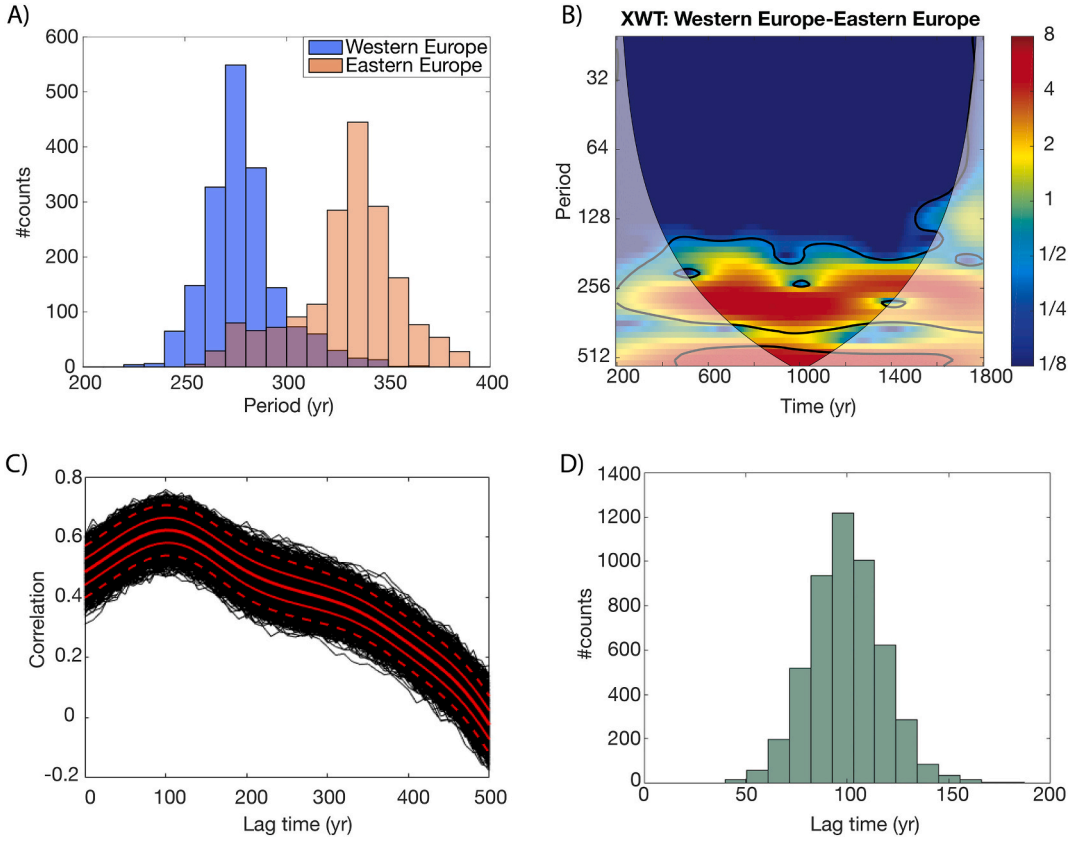

Fig. 7. A) Characteristic period of the PSV curves obtained by application of the empirical mode decomposition method for Western (in blue) and Eastern (in orange) Europe. B) Cross-correlation wavelet analysis for both Western and Eastern curves showing the shared characteristic periods. C) Correlation between the Western and Eastern curves. The mean correlation is given by the thick red line (with error bands at 68% -thin red lines- and 95% -dashed red lines- of confidence). D) Histogram showing the lag-time that corresponds to the maximum correlation obtained in C). Note that for A), B) and D) a Monte-Carlo approach is applied by means of a bootstrap to take into account the error bar of both PSV curves. This method provides a set of 5000 PSV curves whose analysis is reflected in the different plots by the histograms (A and D) and the curves (C). (For interpretation of the references to colour in this figure legend, the reader is referred to the web version of this article.)

range of periods, but showing the higher amplitude (red colors) for a period of about 325 yr (in agreement too with the EDM results) and other period around 550 yr (that can be also seen in the Western curve, but with less significance). To analyze if both wavelets share some periods, we apply a cross-correlation wavelet analysis that combines the previous wavelet results to provide the common periods of both curves. The cross-correlation wavelet is shown in Fig. 7B. Results at 95% of confidence show that the Eastern and Western curves share a common period of about 250–350 yr (supporting the findings of the EMD study) and a higher period of about 550–600 yr that is not significant due to the length of the time window of our analysis.

A second statistical study was carried out to estimate the lag-time between the PSV curves (as visually suggested by the correlation attempted in Fig. 6H). To perform this study, we fix in time the Western curve and move the Eastern curve using lag-times between 0 and 500 yr by steps of 1 yr. As for the previous study, the mean and the error bar at 95% of the PSV curves (Fig. 7C) are taken into account by means of a Monte-Carlo bootstrap. To better determine the lag-time, for each iteration of the bootstrap approach, we keep the lag-time given by the maximum correlation index of that iteration. These selected lag-times follow a normal distribution (Fig. 7D) with which we estimate the mean lag-time and its standard deviation. Results show that the maximum of correlation (about 0.6) provides a systematic lag-time of approx. 100 ± 20 yr, but other possible lag-times are also possible with lower correlation index (see Fig. 7C and D and the right panel of Fig. S1 of the supplementary material).

In summary, our statistical analysis (Fig. 7) suggests that the occurrence of the intensity maxima is characterized by a period of about 300 ± 50 yr for both the Western and the Eastern curves. This result is in agreement with the period of 250 years proposed by Genevey et al. (2016) for Western Europe and that was interpreted as a particular characteristic of the secular variation in the region probably linked to a wave motion in the liquid core (e.g., Finlay and Jackson, 2003; Buffett, 2014). In addition, the lag-time of about 100 yr found between the Eastern and Western curves seems to indicate an eastward drift of a regional intensity patch at the core-mantle boundary beneath Europe that is the responsible of the succession of the intensity maxima observed at the Earth's surface. However, cautions about these results should be considered, since the uncertainties involved in the archeointensity measurements play an important role (from the laboratory experimental to dating and construction of the mean curves) and these findings clearly require further confirmation. The establishment of more robust and precise PSV curves for the different European regions will provide new insights for confirming or not the hypothesis proposed here. For this purpose, the acquisition of robust data from precisely dated archaeological European contexts is crucial.

Supplementary data to this article can be found online at https://doi.org/10.1016/j.pepi.2021.106749.

Author statement

MRM and MGP designed and developed the project, analyzed the paleointensity experiments and wrote the first version of the paper with the help of FJPC, MACO, APO, EA, ET and DK. MRM performed the paleointensity experiments. MRM, APO and ET performed the rock-magnetic experiments and together with FMH and MGP interpreted the results. MRM, FJPC, designed and performed the calculation of the secular variation curves. FJPC performed the statistical analysis. The archaeological team is formed by MACO, LF, CMF, JRT. All authors discussed the results and commented on the manuscript.

Declaration of Competing Interest

The authors declare that they have no known competing financial interests or personal relationships hat could have appeared to influence the work reported in this paper.

Acknowledgments

This research has been funded by the CGL2015-63888-R (PI: M. Gómez-Paccard) and PGC2018-099103-A-I00 (PI: F.J. Pavón-Carrasco) projects and the FPI BES-2016-077257 (MRM) grant of the Ministerio de Ciencia, Innovación y Universidades (Spain). The ceramic samples from the Balearic Islands were obtained in synergy with the project ARCH-REMOTELANDS (HAR2017-83335-P), PI: Miguel Ángel Cau Ontiveros, funded by the Ministerio de Ciencia, Innovación y Universidades, with contribution from the ERDF from the European Commission, and is part of the activities of the ERAAUB, Consolidated Group (2017 SGR 1043), thanks to the support of the Comissionat per a Universitats i Recerca del DIUE de la Generalitat de Catalunya. The authors wish to acknowledge the professional support of the CSIC Interdisciplinary Thematic Platform Open Heritage: Research and Society (PTI-PAIS). All archaeologists are acknowledged for their contribution and guidance during sampling. We extend our warm thanks to our colleagues of the IPGP (Paris), especially to France Lagroix and Jean-Pierre Valet, where the FORCs were performed. The raw data corresponding to this article are available on Magnetics Information Consortium (MagIC) database and can be accessed in the link.

earthref.org/MagIC/17132. The Editors, Dominique Jault, Yves Gallet and Gwenaël Hervé, and reviewers, Ron Shaar and Agnès Genevey, are sincerely acknowledged for their constructive comments on our manuscript.

References

Aidona, E., Polymeris, G.S., Camps, P., Kondopoulou, D., Ioannidis, N., Raptis, K., 2018. Archaeomagnetic versus luminescence methods: the case of an early byzantine ceramic workshop in Thessaloniki, Greece. Archaeol. Anthropol. Sci. 10 (4), 725–741.

Ben-Yosef, E., Tauxe, L., Levy, T.E., Shaar, R., Ron, H., Najjar, M., 2009. Geomagnetic intensity spike recorded in high resolution slag deposit in southern Jordan. Earth Planet. Sci. Lett. 287 (3–4), 529–539.

Brown, M.C., Donadini, F., Korte, M., Nilsson, A., Korhonen, K., Lodge, A., Lengyel, S.N., Constable, C.G., 2015. GEOMAGIA50.v3: 1 General structure and modifi-cations to the archeological and volcanic database. Earth Planets Space 67, 83. https://doi.org/10.1186/s40623–015-0232-0.

Buffett, B., 2014. Geomagnetic fluctuations reveal stable stratification at the top of the earth's core. Nature 507, 484–486. https://doi.org/10.1038/nature13122.

Burlatskaya, S.P., 1970. Change in geomagnetic field intensity in the last 8500 years, according to global archeomagnetic data. Geomagn. Aeron. Engl. Transl. 10, 544–548.

Burlatskaya, S.P., Nachasova, I.E., Didenko, E.J., Shelestun, N.K., 1986. Archeomagnetic Determinations of Geomagnetic Field Elements, Sov. Geophys. Comm. of the USRR Acad. of Sci., Moscow.

Butler, R.F., 1998. Paleomagnetism: Magnetic Domains to Geologic Terranes, Elec-tronic edition, p. 23.

Buxeda Garrigós, J., Cau Ontiveros, M.A., Tuset Bertran, F., 1997. Las cerámicas de la habitación 39 de la basílica de Es Cap de Port (Fornells, Menorca): primeros resultados. In: Comas, M., Gurt, J.M., López, A., Padros, P., Roca, M. (Eds.), Contextos ceràmics d'època romana tardana i de l'alta edat mitjana (segles IV-X). Universitat de Barcelona, pp. 229–248. Arqueo Mediterrània 2/1997.

Buxeda Garrigós, J., Cau Ontiveros, M.A., Gurt Esparraguera, J.M., Tsantini, E., Rauret Dalmau, A.M., 2005. Late Roman coarse and cooking wares from the Balearic Islands in late antiquity. In: Gurt, J.M., Buxeda, J., Cau, M.A. (Eds.), LRCW I: late Roman coarse wares, cooking wares and amphorae in the Mediterranean: archaeology and Archaeometry. BAR international series 1340, Archaeopress, Oxford, pp. 223–254.

Campuzano, S.A., Gómez-Paccard, M., Pavón-Carrasco, F.J., Osete, M.L., 2019. Emergence and evolution of the South Atlantic anomaly revealed by the new paleomagnetic reconstruction SHWQ2k. Earth Planet. Sci. Lett. 512, 17–26.

Cau, M.A., 2003. Cerámica tardorromana de cocina de las Islas Baleares: Estudio arqueométrico, British Archaeological Reports, Internacional Series, 1182. Archaeopress, Oxford.

Cau Ontiveros, M.A., Tsantini, E., Fantuzzi, L., Ramon, J., 2019. Archaeometric characterisation of late antique pottery from the rural site of Ses Païsses de Cala d'Hort (Eivissa, Balearic Islands, Spain). Archaeol. Anthropol. Sci. 11 (2), 627–649.

Chauvin, A., Garcia, Y., Lanos, P., Laubenheimer, F., 2000. Paleointensity of the geomagnetic field recovered on archaeomagnetic sites from France. Phys. Earth Planet. Inter. 120, 111–136.

Coe, R.S., Grommé, S., Mankinen, E.A., 1978. Geomagnetic paleointensities from radiocarbon-dated lava flows on Hawaii and the question of the Pacific nondipole low. J. Geophys. Res. Solid Earth 83 (B4), 1740–1756.

Constable, C., Korte, M., Panovska, S., 2016. Persistent high paleosecular variation activity in southern hemisphere for at least 10 000 years. Earth Planet. Sci. Lett. 453, 78–86.

Day, R., Fuller, M.D., Schmidt, V.A., 1977. Hysteresis properties of titanomagnetites: grain size and composition dependence. Phys. Earth Planet. Inter. 13, 260–266.
De Marco, E., Spatharas, V., Gómez-Paccard, M., Chauvin, A., Kondopoulou, D., 2008. New archaeointensity results from archaeological sites and variation of the geomagnetic field intensity for the last 7 millennia in Greece. Phys. Chem. Earth 33 (6–7), 578–595.
de Palol, P., 1982. La basílica des Cap des Port, de Fornells. Menorca, in II Reunió d'Arqueologia Cristiana Hispànica, 353-404. Institut d'Arqueologia i Prehistòria, Publicacions eventuals, 31, Barcelona.
Donadini, F., Motschi, A., Rösch, C., Hajdas, I., 2012. Combining an archaeomagnetic and radiocarbon study: dating of medieval fireplaces at the Mühlegasse, Zürich. J. Archaeol. Sci. 39 (7), 2153–2166.
Dunlop, D.J., 2002. Theory and application of the Day plot (Mrs/Ms versus Hcr/Hc) 1. Theoretical curves and tests using titanomagnetite data. J. Geophys. Res. Solid Earth 107 (B3). EPM-4.
Egli, R., 2013. VARIFORC: an optimized protocol for calculating non-regular first-order reversal curve (FORC) diagrams. Glob. Planet. Chang. 110, 302–320.
Enkin, R.J., Baker, J., Nourgaliev, D., Iassonov, P., Hamilton, T.S., 2007. Magnetic hysteresis parameters and day plot analysis to characterize diagenetic alter-ation in gas hydrate-bearing sediments. J. Geophys. Res. 112, B06S90. https://doi.org/10.1029/2006JB004638.
Finlay, C.C., Jackson, A., 2003. Equatorially dominated magnetic field change at the surface of the Eath's core. Science 300, 2084–2086.
Flandrin, P., 2009. Matlab Toolbox: Empirical mode decomposition. http://perso.ens-lyon.fr/patrick.flandrin/software2.html.
Gallet, Y., Genevey, A., Le Goff, M., Warme, N., Gran-Aymerich, J., Lefevre, A., 2009. On the use of archeology in geomagnetism, and vice-versa: recent developments in archeomagnetism. Comptes Rendus Physique 10 (7), 630–648.
Genevey, A., Gallet, Y., 2002. Intensity of the geomagnetic field in western Europe over the past 2000 years: new data from ancient French pottery. J. Geophys. Res. 107 (B11), 2285. https://doi.org/10.1029/2001JB000701.
Genevey, A., Gallet, Y., Constable, C.G., Korte, M., Hulot, G., 2008. ArcheoInt: an upgraded compilation of geomagnetic field intensity data for the past ten millennia and its application to the recovery of the past dipole moment. Geochem. Geophys. Geosyst. 9 (4), Q0438.
Genevey, A., Gallet, Y., Rosen, J., Le Goff, M., 2009. Evidence for rapid geomagnetic field intensity variations in Western Europe over the past 800 years from new French archeointensity data. Earth Planet. Sci. Lett. 284 (1–2), 132–143.
Genevey, A., Gallet, Y., Thébault, E., Jesset, S., Le Goff, M., 2013. Geomagnetic field intensity variations in Western Europe over the past 1100 years. Geochem. Geophys. Geosyst. 14 (8), 2858–2872.
Genevey, A., Gallet, Y., Jesset, S., Thébault, E., Bouillon, J., Lefèvre, A., Le Goff, M., 2016. New archeointensity data from French early medieval pottery production (6th–10th century AD). Tracing 1500 years of geomagnetic field intensity variations in Western Europe. Phys. Earth planet. Inter. 257, 205–219.
Genevey, A., Kondopoulou, D., Petridis, P., Aidona, E., Muller, Blonde, Gros, J.S., 2018. New constraints on geomagnetic field intensity variations in the Balkans during the early byzantine period from ceramics unearthed at Thasos and Delphi, Greece. J. Arch. Sci: Reports 21, 952–961.
Genevey, A., Principe, C., Gallet, Y., Clemente, G., Le Goff, M., Fournier, A., Pallecchi, P., 2019. Refining the High-Fidelity Archaeointensity Curve for Western Europe over the Past Millennium: Analysis of Tuscan Architectural Bricks (Italy). Geological Society., London, Special Publications.
Gómez-Paccard, M., Chauvin, A., Lanos, P., Thiriot, J., Jiménez-Castillo, P., 2006. Archeomagnetic study of seven contemporaneous kilns from Murcia (Spain). Phys. Earth Planet. Inter. 157 (1–2), 16–32.
Gómez-Paccard, M., Chauvin, A., Lanos, P., Thiriot, J., 2008. New archeointensity data from Spain and the geomagnetic dipole moment in western Europe over the past 2000 years. J. Geophys. Res. 113, B09103 https://doi.org/10.1029/2008JB005582.
Gómez-Paccard, M., Chauvin, A., Lanos, P., Dufresne, P., Kovacheva, M., Hill, M.J., Beamud, E., Blain, S., Bouvier, A., Guibert, P., Archaeological Working Team, 2012. Improving our knowledge of rapid geomagnetic field intensity changes observed in Europe between 200 and 1400 AD. Earth Planet. Sci. Lett. 355–356, 131–143.
Gómez-Paccard, M., Osete, M.L., Chauvin, A., Pavón-Carrasco, F.J., Pérez-Asensio, M., Jiménez, P., Lanos, P., 2016. New constraints on the most significant paleointensity change in Western Europe over the last two millennia. A non-dipolar origin? Earth planet. Sci. Lett. 454, 55–64.
Gómez-Paccard, M., Chauvin, A., Albeck, M.E., Zaburlín, M.A., Basso, D.M., Pavón-Carrasco, F.J., Osete, M.L., Campuzano, S.A., 2019. New archeointensity data from NW Argentina (1300-1500 CE). Phys. Earth Planet. Inter. 286, 92–100.
Gurt, J.M., 2007. Complejos eclesiásticos no episcopales función y gestión. In: Quiroga, J. L., Tejera, A.M. Martínez, de Pablos, J. Morín (Eds.), Monasteria et territoria. Elites, edilicia y territorio en el Mediterraneo medieval (siglos V–XI): Actas del III Encuentro Internacional e Interdisciplinar sobre la alta Edad Media en la Península Ibérica (Madrid 2007), pp. 203–232.
Hedley, I.G., Wagner, J.-J., 1991. A magnetic investigation of Roman and pre-Roman pottery. In: Pernicka, E., Wagner, G.A. (Eds.), Archaeometry'90. Springer, New York, pp. 275–284 edited by.
Hervé, G., Chauvin, A., Lanos, P., Rochette, P., Perrin, M., Perron d'Arc, M., 2019. Cooling rate effect on thermoremanent magnetization in archaeological baked clays: an experimental study on modern bricks. Geophys. J. Int. 217 (2), 1413–1424.
Jasonov, P.G., Nourgaliev, D.K., Burov, B.V., Heller, F., 1998. A modernized coercivity spectrometer. Geol. Carpath. 49 (3), 224–226.
Kirschvink, J.L., 1980. The least-squares line and plane and the analysis of palaeomagnetic data. J. R. Astron. Soc. 62 (3), 699–718.
Kondopoulou, D., Aidona, E., Ioannidis, N., Polymeris, G.S., Tsolakis, S., 2015. Archaeomagnetic study and thermoluminescence dating of Protobyzantine kilns (Megali Kypsa, North Greece). J. Archaeol. Sci. Rep. 2, 156–168.
Kontny, A., Grothaus, L., 2017. Effects of shock pressure and temperature on titanomagnetite from ICDP cores and target rocks of the El'gygytgyn impact structure, Russia stud. Geophys. Geod. 61, 163–183.
Kovacheva, M., Boyadziev, Y., Kostadinova-Avramova, M., Jordanova, N., Donadini, F., 2009. Updated archeomagnetic data set of the past eight millenia from the Sofia laboratory, Bulgaria. Geochem. Geophys. Geosyst. 10, Q05002 https://doi.org/10.1029/2008GC002347.
Kovacheva, M., Kostadinova-Avramova, M., Jordanova, N., Lanos, P., Boyadzhiev, Y., 2014. Extended and revised archaeomagnetic database and secular variation curves from Bulgaria for the last eight millennia. Phys. Earth Planet. Inter. 236, 79–94.
Livermore, P.W., Fournier, A., Gallet, Y., Bodin, T., 2018. Transdimensional inference of archeomagnetic intensity change. Geophys. J. Int. 215 (3), 2008–2034.
López-Sánchez, J., Palencia-Ortas, A., del Campo, A., McIntosh, G., Kovacheva, M., Martín-Hernández, F., Carmona, N., Rodríguez de la Fuente, O., Marín, P., Molina-Cardín, A., Osete, M.L., 2020. Further progress in the study of epsilon iron oxide in archaeological baked clays. Phys. Earth Planet. Inter. 307, 106554.
Lowrie, W., 1990. Identification of ferromagnetic minerals in a rock by coercivity and unblocking temperature properties. Geophys. Res. Lett. 17, 159–162. https://doi.org/10.1029/GL017i002p00159.
Mas Florit, C., Vallori, B., Murrieta, P., Rivas, M.J., Cau, M.A., 2015. The Roman Villa of Sa Mesquida: A Rural Settlement on the Island of Mallorca (Balearic Islands, Spain). In: Militello, P.M., Öniz, H. (Eds.), SOMA 11, Proceedings of the 15th Symposium on Mediterranean Archaeology, Held at the University of Catania 3–5 March 2011, BAR, International Series, 2695, vols. I. Archaeopress, Oxford, pp. 461–466.
Mas Florit, C., Cau Ontiveros, M.A., Alcaide, S., 2020. Buildings of faith: early Christianity in the countryside of the Balearics (Spain). J. Roman Archaeol. 33, 271–290.
Molina-Cardín, A., Campuzano, S.A., Osete, M.L., Rivero-Montero, M., Pavón-Carrasco, F.J., Palencia-Ortas, A., Martín-Hernández, F., Gómez-Paccard, M., Chauvin, A., Guerrero-Suárez, S., Pérez-Fuentes, J.C., McIntosh, G., Catanzariti, G., Sastre-Blanco, J.C., Larrazabal, J., Fernández-Martínez, V.M., Álvarez-Sanchís, J.R., Rodríguez-Hernández, J., Martín-Viso, I., García, I., Rubert, D., 2018. Updated Iberian archeomagnetic catalogue: new full vector paleosecular variation curve for the last three millennia. Geochem. Geophys. Geosyst. 19, 3637–3656. https://doi.org/10.1029/2018GC007781.
Ogishima, T., Morijiri, R., Ueno, N., 2000. Measurement of archeomagnetic intensity of bricks from a Roman ruin in Slovakia. Bull. Geophys. Surv. Jpn. 51, 237–249.
Orfila, M., Cau, M.A., 1994. Las cerámicas finas procedentes de la cisterna de Sa Mesquida, Calvià (Mallorca), in III Reunió d'Arqueologia Cristiana Hispànica, Maó, 12–17 de setembre de 1988, Monografies de la Secció Històrico-Arqueològica. Institut d'Estudis Catalans, Barcelona, pp. 257–288.
Pantò, G., Vaschetti, L., 2010. Fornaci e ceramisti a Chieri fra XIII e XVI secolo. In: Atti XLII Convegno Internazionale della Ceramica in Età Medievale e Moderna, pp. 147–158.
Paterson, G.A., Tauxe, L., Biggin, A.J., Shaar, R., Jonestrask, L.C., 2014. On improving the selection of Thellier-type paleointensity data. Geochem. Geophys. Geosyst. 15 (4), 1180–1192.
Pavón-Carrasco, F.J., Gómez-Paccard, M., Hervé, G., Osete, M.L., Chauvin, A., 2014. Intensity of the geomagnetic field in Europe for the last 3 ka: influence of data quality on geomagnetic field modeling. Geochem. Geophys. Geosyst. 15. https://doi.org/10.1002/2014GC005311.
Pavón-Carrasco, F.J., Campuzano, S.A., Rivero-Montero, M., Molina-Cardín, A., Gómez-Paccard, M., Osete, M.L., 2021. SCHA. DIF. 4k: 4000 years of paleomagnetic reconstruction for Europe and its application for dating. J. Geophys. Res. Solid Earth 126 (3) e2020JB021237.
Pesonen, L.J., Leino, M.A.H., Nevanlinna, H., 1995. Archaeomagnetic intensity in Finland during the last 6400 years: evidence for a latitude-dependent nondipole field at~ AD 500. J. Geomagn. Geoelectr. 47 (1), 19–40.
Pick, T., Tauxe, L., 1993. Holocene paleointensities: Thellierexperiments on subma-rine basaltic glass from the East Pacific Rise. J. Geophys. Res. Solid Earth 98 (B10), 17949–17964.
Ramon, J., 1986. El Baix imperi i l'època bizantina a les Illes Pitiüses. Consell Insular d'Eivissa i Formentera, Ibiza.
Ramon, J., 1994. Ses Països de cala d'Hort: Un establiment rural d'época antiga al sud¬oest d'Eivissa, in Quaderns d'Arqueologia Pitiüsa, volúmen I, Conselleria de Cultura. Consell Insular d'Eivissa i Formentera, Eivissa.
Ramon, J., 1995. Ses Païsses de Cala d'Hort: un establiment rural d'època antiga al sud-oest d'Eivissa. In: Conselleria de Cultura. Formentera, Eivissa, Consell Insular d'Eivissa i.
Ramon, J., 2008. La cerámica ebusitana en la Antigüedad Tardía. In: Bernal, D., Ribera, A. (Eds.), Cerámicas hispanorromanas: un estado de la cuestión. Servicio de Publicaciones de la Universidad de Cádiz, Cádiz, pp. 563–583.
Ramon, J., Cau, M.A., 1997. Niveles de época vándala de Es Castell d'Eivissa, in Contextos ceràmics d'època romana tardana i de l'alta edat mitjana (segles IV-X). In: Comas, M., Gurt, J.M., López, A., Padros, P., Roca, M. (Eds.), ArqueoMediterrània, 2. Universitat de Barcelona, pp. 269–311.
Ripoll, G., Carrero, E., Rico, D., Tuset, F., Velázquez, I., López Batlle, A., Mas, C., Valls, M., Cau, M.A., 2012. La arquitectura religiosa hispánica del siglo IV al X y el proyecto del Corpus Architecturae Religiosae Europeae – CARE-Hispania. Hortus Artium Medievalium 18, 45–73.
Rivero-Montero, M., Gómez-Paccard, M., Kondopoulou, D., Tema, E., Pavón-Carrasco, F. J., Aidona, E., Campuzano, S.A., Molina-Cardín, A., Osete, M.L., Palencia-Ortas, A., Martin-Hernándes, F., Rubat-Borel, F., Venturino, M., 2021. Geomagnetic field

intensity changes in the Central Mediterranean between 1500 BCE and 150 CE: implications for the Levantine Iron age anomaly evolution. Earth Planet. Sci. Lett. 557, 116732. https://doi.org/10.1016/j.epsl.2020.116732.
Roberts, A.P., Pike, C.R., Verosub, K.L., 2000. First-order reversal curve diagrams: a new tool for characterizing the magnetic properties of natural samples. J. Geophys. Res. Solid Earth 105 (B12), 28461–28475.
Schnepp, E., Brüggler, M., 2016. Archaeomagnetic investigation of a Roman glass workshop in Goch-Asperden, Germany. J. Archaeol. Sci. Rep. 10, 322–330.
Schnepp, E., Thallner, D., Arneitz, P., Leonhardt, R., 2020. New archeomagnetic secular variation data from Central Europe. II: Intensities. Phys. Earth Planet. Inter. 309, 106605.
Sdrolia, S., 2016. Habitation in the region of Mount Ossa during the early byzantine period. Archaeological Reports 62, 125–132.
Shaar, R., Ben-Yosef, E., Ron, H., Tauxe, L., Agnon, A., Kessel, R., 2011. Geomagnetic field intensity: how high can it get? How fast can it change? Constraints from Iron age copper slag. Earth Planet. Sci. Lett. 301 (1–2), 297–306.
Shaar, R., Tauxe, L., Ron, H., Ebert, Y., Zuckerman, S., Finkelstein, I., Agnon, A., 2016. Large geomagnetic field anomalies revealed in bronze to Iron age archeomagnetic data from Tel Megiddo and Tel Hazor, Israel. Earth Planet. Sci. Lett. 442, 173–185.
Spassov, S., Hus, J., Geeraerts, R., Heller, F., 2008. Archaeomagnetic dating of a high middle age likely iron working site in Corroy-le-grand (Belgium). Physics and Chemistry of the Earth, Parts A/B/C 33 (6–7), 544–556.
Spatharas, V., Kondopoulou, D., Aidona, E., Efthimiadis, K.G., 2011. New magnetic mineralogy and archaeointensity results from Greek kilns and baked clays. Stud. Geophys. Geod. 55 (1), 131–157.
Tema, E., Goguitchaichvili, A., Camps, P., 2010. Archaeointensity determinations from Italy: new data and the Earth's magnetic field strength variation over the past three millennia. Geophys. J. Int. 180 (2), 596–608.
Tema, E., Gómez-Paccard, M., Kondopoulou, D., Almar, Y., 2012. Intensity of the Earth's magnetic field in Greece during the last five millennia: new data from Greek pottery. Phys. Earth Planet. Inter. 202, 14–26.
Tema, E., Camps, P., Ferrara, E., Poidras, T., 2015. Directional results and absolute archaeointensity determination by the classical Thellier and the multi-specimen DSC protocols for two kilns excavated at Osterietta, Italy. Stud. Geophys. Geod. 59 (4), 554–577.
Tema, E., Ferrara, E., Angelici, D., Fantino, F., Panero, E., 2019. The importance of multidisciplinary dating in rescue excavations: the case of Santhià, northern Italy. J. Archaeol. Sci. Rep. 28, 102059.
Thébault, E., Gallet, Y., 2010. A bootstrap algorithm for deriving the archeomagnetic field intensity variation curve in the Middle East over the past 4 millennia BC. Geophys. Res. Lett 37, 22.
Thellier, E., Thellier, O., 1959. Sur l'intensité du champ magnétique terrestre dans le passé historique et géologique. Ann. Géophys 15, 285–376.